© Indian Academy of Sciences

REGULAR ARTICLE

Experimental and computational analysis (DFT method) of some quinoxalinones and benzoxazinones: spectroscopic investigation (FT-IR, FT-Raman, UV-Vis, NMR)

JELENA PETRONIJEVIĆ[a,*], NENAD JOKSIMOVIĆ[a], ZORICA BUGARČIĆ[a], ELVIRA ĐURĐIĆ[b] and NENAD JANKOVIĆ[a,*]

[a]Department of Chemistry, Faculty of Science, University of Kragujevac, Radoja Domanovića 12, Kragujevac 34000, Serbia
[b]Department of Physics, Faculty of Science, University of Novi Sad, Trg Dositeja Obradovica 4, Novi Sad 21000, Serbia
E-mail: jelena.petronijevic@pmf.kg.ac.rs; nenad.jankovic@kg.ac.rs

Abstract. The selected quinoxalinones and benzoxazinones derivatives, synthesized in our laboratory earlier, were explored by spectroscopic techniques (UV-Vis, IR, Raman and NMR) and theoretical study (DFT calculations). In order to understand the electronic properties of these compounds, the theoretical UV spectra have been investigated by TDDFT/B3LYP method with 6-311+G(d,p) basis set in ethanol as a solvent. For all compounds, the absorption of UV radiation with a wavelength around 415 nm with an oscillator strength f = 0.90 induces the intramolecular electronic transition (n→π*). The frontiers molecular orbitals are calculated, and contributions of the electronic transitions are determined. Also, we did quantum chemical calculations to investigate the corrosion inhibition properties of these molecules. The vibrational analysis was performed at the B3LYP/6-311+G(d,p) level of theory *in vacuo*. Obtained results are in very good agreement with experimental data. The calculated ^{13}C NMR shifts in all cases are in good-to-excellent agreement. Also, ^{1}H NMR predicted shifts are comparable with experimental results, but there are some deviations (for N–H shifts) probably as a consequence of intramolecular interactions.

1. Introduction

The quinoxaline and benzoxazine derivatives are mainly known for their wide range of pharmacological and biological activities.[1–3] Their ring moieties are part of the chemical structures of various antibiotics such as echinomycin, levomycin and actinomycin.[2] Such compounds are also known to be active against transplant tumors.[4] Also, quinoxaline-based compounds have the ability to inhibit the metal corrosion and they are used in electroluminescent materials.[5,6] Physicochemical properties of inhibitors (e.g., electron density, geometric factors, molecular volume, etc.,) determine their effectiveness of corrosion, while the process of adsorption depends on the type of metal, the nature of inhibitor, and the electrochemical potential at the metal-solution surface.[7] Many quinoxaline derivatives have been reported as efficient inhibitors of metal corrosion in acidic medium in the last few years.[8–12] Nowadays, many scientists and engineers are investigating new synthetic routes for the synthesis of novel corrosion inhibitors with even better properties. There are numerous methods available for the synthesis of quinoxaline and benzoxazine derivatives. In recent times, several green methodologies that include recyclable catalysts, microwave-assisted synthesis and reactions in aqueous medium are presented.[13,14] Bearing in mind the biological, structural, and industrial importance of quinoxaline- and benzoxazine-based compounds, we used these previously

*For correspondence

Published online: 05 November 2019

synthesized compounds for DFT calculations.[13] The studied quinoxaline and benzoxazine derivatives namely 3,4-dihydro-3-[2-oxo-2-(4-methoxyphenyl) ethylidene]-2(1H)-quinoxalinone (**1**), 3,4-dihydro-3-(5-methyl-2-oxo-hex-5-enylidene)-2(1H)-quinoxalinone (**2**), 3,4-dihydro-3-[2-oxo-2-(3-nitrophenyl)ethylidene] -2(1H)-quinoxalinone (**3**) and 3,4-dihydro-3-[2-oxo-2-(3-N-acetylphenyl)ethylidene]-1,4-benzoxazin-2-one (**4**) are presented in Figure 1. In this study, the equilibrium conformation of selected compounds was predicted theoretically using B3LYP/6-311+G(d,p) level of theory. Obtained optimized structural parameters are compared with crystal structure data of similar molecular structure. In order to investigate the corrosion inhibition properties of these molecules we calculated quantum chemical parameters. The complete assignments were performed on the recorded FT-IR spectrum based on theoretically predicted wavenumbers and their TED. The calculated vibrational frequencies are scaled to compensate for the approximate treatment of electron correlation, for basis set deficiencies and for the anharmonicity.[15,16] The electronic transitions and isotropic chemical shifts were analyzed *via* UV-Vis and ^{1}H and ^{13}C NMR techniques. We have carried out DFT calculations with the combined Becke's three-parameter exchange functional in combination with the Lee, Yang and Parr correlation functional (B3LYP).[17–19] Computational techniques

can facilitate the solution of the problems confronted in experimental chemistry.

2. Experimental and theoretical calculations

2.1 *Experimental*

The synthesis of the selected compounds was previously reported by our investigation group.[13] All solvents were purchased from Sigma Aldrich and used without purification. UV spectra (c = 1.0 × 10^{-4} mol dm^{-3}, path length 1 cm) were measured in ethanol as solvent, in the wavelength range of 200–600 nm using a Perkin Elmer Lambda 35 double-beam spectrophotometer at 25 °C. The IR spectra were recorded *via* Perkin-Elmer Spectrum One FT-IR spectrometer on a KBr pellet in the range of 400–4000 cm^{-1}. Raman spectra were collected using Thermo Fisher Scientific DXR Raman Microscope at 25 °C. This device uses DPSS (Diode Pumped Solid State) lasers with wavelength λ = 780 nm. The laser used for the excitation is coupled with the optical Olympus microscope and objective with 10 magnification, which focuses the laser beam onto the sample. Through the same microscope objective and pinhole aperture with diameter of 50 μm, Raman backscattered data was collected with CCD camera as a detector. The recorded wavenumbers are expected to be accurate within ±4 cm^{-1} in the range of 50–3395 cm^{-1}. OMNIC software was used for collecting and analyzing the obtained Raman spectra of the samples. The NMR spectra
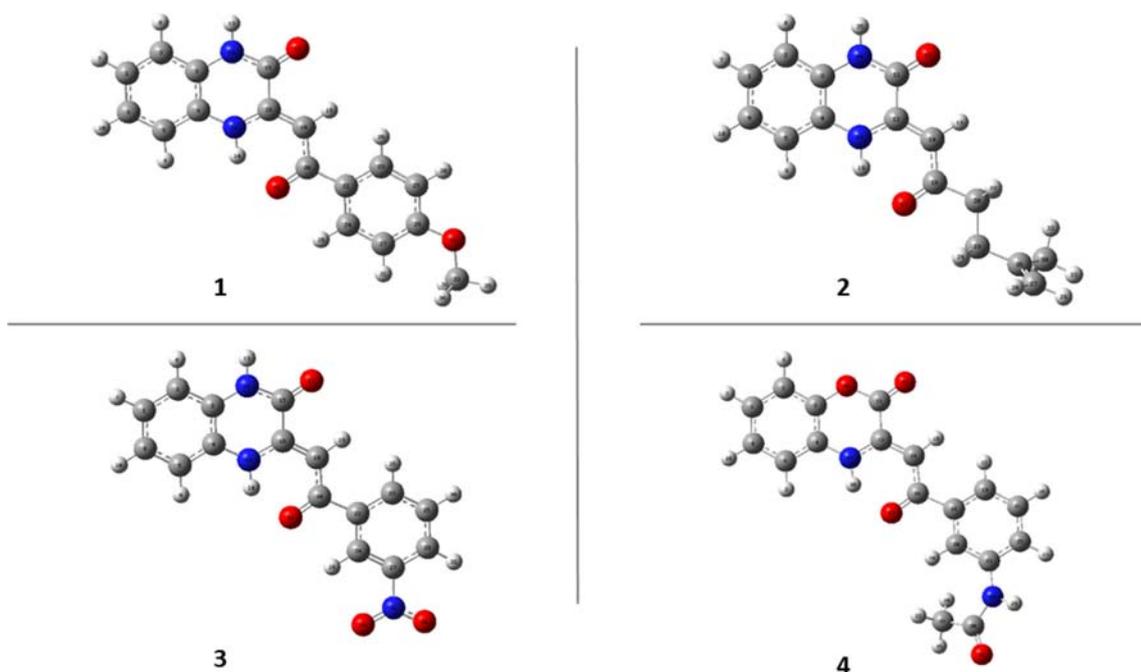
Figure 1. Optimized structures of investigated compounds.

of the evaluated compounds have been performed in DMSO-d$_6$ with TMS as the internal standard on a Varian Gemini 200 MHz NMR spectrometer (^{1}H at 200 and ^{13}C at 50 MHz). Physical properties of compound **1**: orange powder, M.p. = 241 °C; compound **2**: orange powder, M.p. > 300 °C; compound **3**: orange powder, M.p. > 300 °C; compound **4**: yellow powder, M.p. = 235 °C.

2.2 *Computational details*

All optimizations of geometries were performed using the density functional theory (DFT) at the B3LYP functional (Becke's Three Parameter Hybrid Functional using the Lee-Yang-Parr correlation functional).[18,19] Calculations were performed using the 6-311+G(d,p)[20] basis set using GAUSSIAN 09 package.[21] In this work, the B3LYP/6-311+G(d,p) theoretical model was used to obtain the ground state geometries of selected quinoxalinones and oxazinones *in vacuo*. Frequency calculations showed that there were no imaginary frequencies, which indicates that the stationary points correspond to the equilibrium geometries. The calculated molecular geometry was used as an input structure for further calculations (UV-Vis, IR, Raman, ^{1}H and ^{13}C NMR spectra). For better understanding of electronic properties, the theoretical UV spectra have been calculated by TDDFT/B3LYP method with 6-311+G(d,p) basis set in ethanol as a solvent. The optimized molecular structures *in vacuo* are used for the computation of vibrational frequencies and Raman activities. Calculated vibrational frequencies were scaled down using a single scaling factor of 0.9679.[22] Quantum chemical properties are also investigated in order to determine corrosion inhibition of selected compounds. The ^{1}H and ^{13}C NMR isotropic chemical shifts were calculated using the GIAO method with DMSO as a solvent.[23] The ^{1}H and ^{13}C NMR chemical shifts of TMS in DMSO were also calculated at the B3LYP/6-311+G(d,p) level of theory and they equal 32.0121 and 184.5363 ppm, respectively. Calculated chemical shifts were scaled using scaling factors of 0.9409 (^{13}C) and 1.1119 (^{1}H), that are obtained using the least squares method.

3. Results and Discussion

3.1 *Molecular geometry*

The optimized structural parameters of the molecule **2** are obtained from B3LYP/6-311+G(d,p) level of theory, and listed in Table 1. The crystal structure of compound **2** is not obtained so we compared the optimized structure with a similar system for which the X-ray data have been obtained, for example, 3,4-dihydro-3-(2-oxo-hex-5-enylidene)-1,4-benzoxazin-2-one.[13] Heterocycle ring of compound **2**, that is part of

two tethered six-membered rings is almost ideally planar that is confirmed for the crystal structure of similar compound 3,4-dihydro-3-(2-oxo-hex-5-enyli-dene)-1,4-benzoxazin-2-one. Calculated dihedral angle of 0.12° between N(18)-C(12)-C(14)-C(16) and dihedral angle of 176,71° between C(14)-C(16)-C(20)-C(23) indicate that all atoms in the molecule (except for the terminal C26–C27–C30 fragment) are part of a large planar system.

Planar conformation of the almost whole system is probably stabilized by a relatively strong intramolecular hydrogen bond, such as N–H···O [H···O = 2.01 Å, N–H···O = 134°].[13] As can be seen in Table 1, theoretical configurations do not match completely with the XRD values. The reason for the deviation is that these calculations refer to the equilibrium structure of an isolated molecule in the gas phase and the experimental results belong to another similar molecule in the condensed phase.

3.2 *Vibrational analysis*

In order to obtain the spectroscopic data for selected compounds we computed harmonic vibrational frequencies using the B3LYP/6-311+G(d,p) level of theory *in vacuo* and the results are listed in Table 2. There are some disagreements between calculated and experimental vibrational wavenumbers because calculations were made *in vacuo*, but experiments were performed for solid-state. The calculated vibrational frequencies were scaled-down with a scaling factor of 0.9679. Based on the calculated normal mode frequencies, the theoretical IR and Raman spectra were convoluted, and it was compared with the experimental FT-IR spectra in Figures 2 and 3 for compounds **1**, **2**, **3** and **4**. The calculated vibrational wavenumbers (ν_{calc}) correlate very well with the experimental data (ν_{exp}) with the correlation equation $\nu_{calc} = 1.0318 \cdot \nu_{exp} - 71.069$ and the correlation coefficient (r^2) of 0.9993 for compound **1**. The assignments of selected modes with TED contributions are given in Table 2. The various functional group analysis was discussed as below.

3.2a *C–H vibrations*: The C–H stretching vibrations of aromatic and aliphatic compounds occur in the ranges of 3100–3000 and 3000–2840 cm^{-1}, respectively.[23] The calculated aromatic C–H stretching vibrations were found to be at 3097, 3085, and 3070 cm^{-1} for the C–H bonds of the aromatic ring bearing quinoxalinone scaffold in all cases, and at 3107, 3094 and 3080 cm^{-1} for the C–H bonds of the

Table 1. The computed geometric parameters of compound **2** and comparison with available experimental results for a similar compound, bond lengths in angstrom (Å) and bond angles in degrees (°).
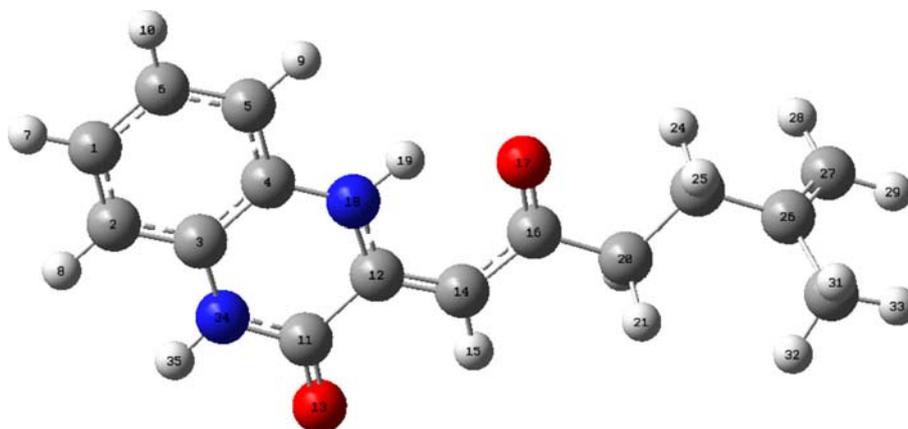
Bond lengths	B3LYP/6−311+G(d,p)	Exper.[13]	Bond angles	B3LYP/6−311+G(d,p)
C(1)-C(2)	1.391		C(2)-C(1)-C(6)	120.1
C(1)-C(6)	1.397		C(1)-C(2)-C(3)	119.9
C(2)-C(3)	1.395		C(2)-C(3)-C(4)	120.1
C(3)-C(4)	1.404	1.386	C(2)-C(3)-N(34)	122.2
C(3)-N(34)	1.397	1.384	C(4)-C(3)-N(34)	117.7
C(4)-C(5)	1.398		C(3)-C(4)-C(5)	119.6
C(4)-N(18)	1.385	1.382	C(3)-C(4)-N(18)	118.5
C(5)-C(6)	1.389		C(5)-C(4)-N(18)	121.9
C(11)-C(12)	1.502	1.494	C(4)-C(5)-C(6)	120.0
C(11)-O(13)	1.217	1.193	C(1)-C(6)-C(5)	120.2
C(11)-N(34)	1.376		C(12)-C(11)-O(13)	123.1
C(12)-C(14)	1.370	1.351	C(12)-C(11)-N(34)	114.9
C(12)-N(18)	1.364	1.357	O(13)-C(11)-N(34)	122.0
C(14)-C(16)	1.447	1.444	C(11)-C(12)-C(14)	119.2
C(16)-O(17)	1.242	1.238	C(11)-C(12)-N(18)	117.7
C(16)-C(20)	1.521	1.493	C(14)-C(12)-N(18)	123.1
C(20)-C(23)	1.534	1.526	C(12)-C(14)-C(16)	122.6
C(23)-C(26)	1.512	1.473	C(14)-C(16)-O(17)	122.5
C(26)-C(27)	1.335	1.351	C(14)-C(16)-C(20)	116.9
C(26)-C(30)	1.509		O(17)-C(16)-C(20)	120.6
			C(4)-N(18)-C(12)	125.1
			C(16)-C(20)-C(23)	113.5
			C(20)-C(23)-C(26)	113.1
			C(23)-C(26)-C(27)	121.6
			C(23)-C(26)-C(30)	116.5
			C(27)-C(26)-C(30)	121.9
			C(3)-N(34)-C(11)	126.1

phenyl ring that is part of benzoyl fragment (for compounds **1**, **3** and **4**). Experimental values for aromatic C–H stretching were found to be at 3143, 3037 and 2963 cm^{-1} for the C–H bonds of the aromatic ring bearing quinoxalinone scaffold in all cases, and at 3143, 3043 and 3002 cm^{-1} for the C–H bonds of the phenyl ring that is part of benzoyl fragment.

The aliphatic C–H stretching vibrations of the methoxy group were calculated at 3046, 2989 and 2926 cm^{-1} for compound **1**, vibrations of the methyl group for compound **2** were calculated at 3033, 3010 and 2900 cm^{-1} and the C-H stretching vibrations of methyl group for compound **4** were calculated at 3055, 2995 and 2937 cm^{-1}. Experimental values for aliphatic C-H stretching were found to be 2965, 2854 and 2811 cm^{-1} for compounds **1**, **2** and **4**.

3.2b *C–C vibrations*: For heteronuclear aromatic compounds, the stretching vibrations of the C–C bonds

Table 2. Comparison of the selected calculated and experimental vibrational modes and proposal assignments of compound **1**.

Unscaled (cm^{-1})	Scaled (cm^{-1})	Observed frequencies		Vibrational assignments (TED%)
		FT-IR	FT-Raman	
3572	3457	3437		$\nu N_{11}H_{13}(79)$
3327	3220			$\nu N_{12}H_{14}(70)$
3252	3147			$\nu C_{18}H_{19}(64)$
3210	3107			$\nu C_{24}H_{28}(30) + \nu C_{27}H_{31}(45)$
3200	3097			$\nu C_1H_7(28) + \nu C_6H_{10}(28) + \nu C_5H_9(13) + \nu C_2H_8(10)$
3199	3096		3079	$\nu C_{23}H_{26}(38)$
3195	3092			$\nu C_{24}H_{28}(43) + \nu C_{27}H_{31}(28)$
3189	3086			$\nu C_1H_7(25) + \nu C_6H_{10}(19) + \nu C_5H_9(25) + \nu C_2H_8(15)$
3184	3081			$\nu C_{23}H_{26}(28) + \nu C_{25}H_{30}(42)$
3178	3076			$\nu C_5H_9(33) + \nu C_6H_{10}(24) + \nu C_2H_8(21)$
3172	3070	3037		$\nu C_1H_7(21) + \nu C_6H_{10}(14) + \nu C_5H_9(11) + \nu C_2H_8(34)$
3147	3046	3002		$\nu C_{33}H_{35}(53) + \gamma C_{33}H_{36}(13) + \gamma C_{33}H_{34}(13)$
3089	2989	2965		$\nu_{asym} C_{33}H_{34}H_{36}(40)$
3023	2926			$\nu_{sym} C_{33}H_{34}H_{36}(36)$
1720	1664	1681	1628	$\nu C_{15}O_{17}(15)$
1610	1558	1597	1580	$\nu(C\text{–}C)_{aromatic}$
1529	1479	1518	1553	$\beta C_4N_{12}C_{16}(6) + \beta C_3N_{11}C_{15}(6)$
1500	1451	1510		$\beta C_{33}H_{34}H_{36}(23) + \beta C_{33}H_{35}H_{36}(12)$
1498	1449	1500		$\nu C_1C_2 + \nu C_1C_6 + \nu C_5C_6 + \nu C_5C_4(6) + \beta C_{29}O_{32}C_{33}(10)$
1493	1445	1445	1445	$\nu C_{33}H_{35}(24) + \gamma C_{33}H_{36}(21)$
1488	1440	1436	1424	$\beta C_{16}C_{18}H_{19}(6) + \beta C_{16}C_{18}C_{20}(6)$
1468	1420	1416	1410	$\beta C_{33}H_{34}H_{36}(9)$
1442	1395		1392	$\beta H_{13}N_{11}C_{15}$
1385	1340	1373	1320	$\beta C_{15}C_{16}N_{12}(6) + \beta C_{18}C_{16}N_{12}(6)$
1181	1143			$\beta C_1C_6H_{10}(11) + \beta C_6C_1H_7(11) + \beta C_5C_6H_{10}(11) + \beta C_2C_1H_7(11)$
1161	1123	1155		$\gamma C_{33}H_{34}(20) + \gamma C_{33}H_{36}(21)$
1052	1018			$\nu C_1C_6(11)$
1034	1000			$\nu C_{32}C_{33}(21)$

were found to be in the narrow ranges of 1600–1585 and 1500–1400 cm^{-1}.[24] Vibrations of aromatic C–C bond that are calculated have values around 1558 and 1340 cm^{-1}. Experimental vibrations are 1553 and 1351 cm^{-1}. As can be seen, matching between experimental and calculated values are excellent. The stretching vibrations of aliphatic C–C bonds for compound **2** were calculated at 1412 cm^{-1} and it was assigned to the band at 1380 cm^{-1} in the experimental FT-IR spectrum.

3.2c *N–H vibrations*: For N–H stretching vibration is found to be in the region of 3300–3500 cm^{-1}.[25] N–H stretching vibrations for compound **1** were calculated at 3457 and 3220 cm^{-1}, for compound **2** at 3472 and 3070 cm^{-1}, for compound **3** at 3460 and 3191 cm^{-1} and for compound **4** at 3480 and 3455 cm^{-1}. These values have a good match with

experimental values that are 3473 (**1**), 3412 (**2**), 3438 and 3411 (**3**) and 3484 cm^{-1} (**4**). Also, in experimental spectra there are no two values for N–H stretching (except for compound **3**) but only one broad band.

3.2d *C=O vibrations*: Carbonyl (C=O) group stretching vibration is expected to appear in the region of 1680–1715 cm^{-1}.[26] For quinoxalinones (**1**, **2**, **3**) amide carbonyl group stretching vibration appear around 1700 cm^{-1} as a strong band in experimental spectra. The calculated value for this stretching vibration is around 1690 cm^{-1}. For oxazinone (**4**) ester carbonyl group stretching vibration appear at 1754 cm^{-1} in experimental spectrum. The value of $\nu_{C=O}$ band is calculated at 1756 cm^{-1}. Experimental values for carbonyl group stretching vibration from benzoyl fragment for all tested compounds are in range of 1605–1650 cm^{-1}.
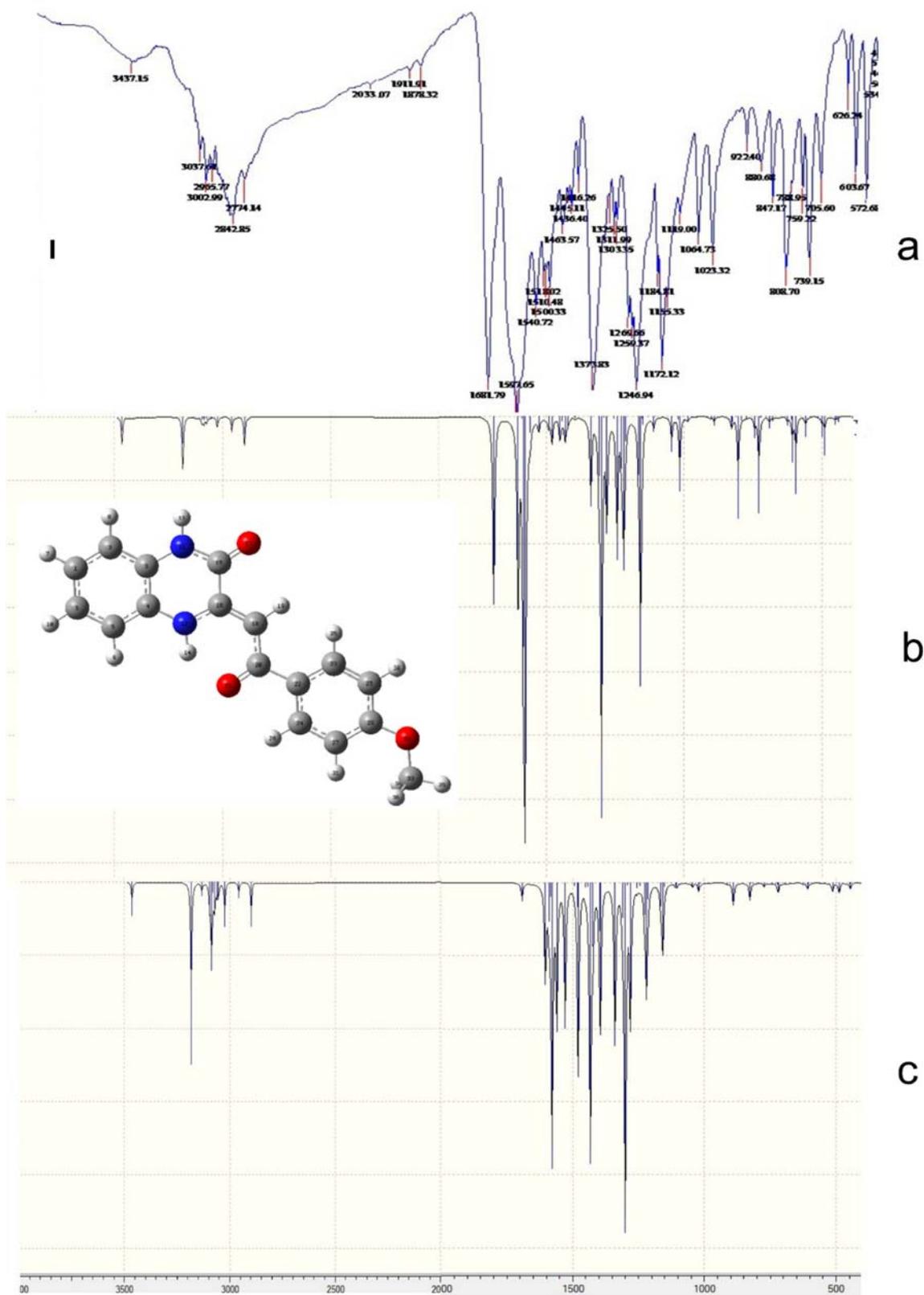
Figure 2. Experimental (a), calculated IR (b) and calculated Raman (c) for compound **1** (picture I) and compound **2** (picture II).

Figure 2. continued
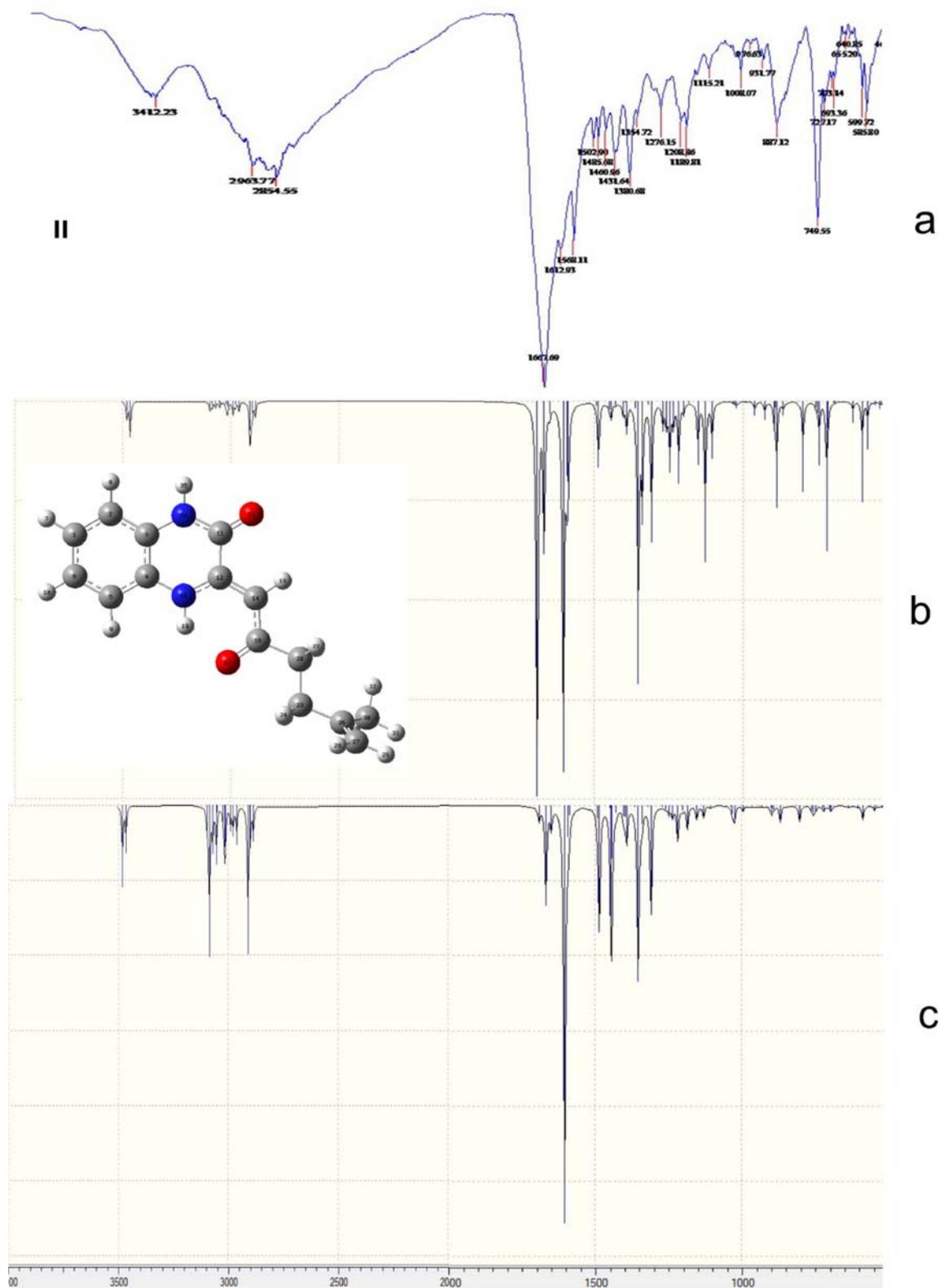
Calculated values are in the range of 1600–1680 cm^{-1}. The value of $\nu_{C=O}$ band from NHCOCH$_3$ fragment (compound **4**) has an experimental value 1599 cm^{-1} and calculated value is 1645 cm^{-1}. Experimental and calculated values of C=O stretching vibration are perfectly match.
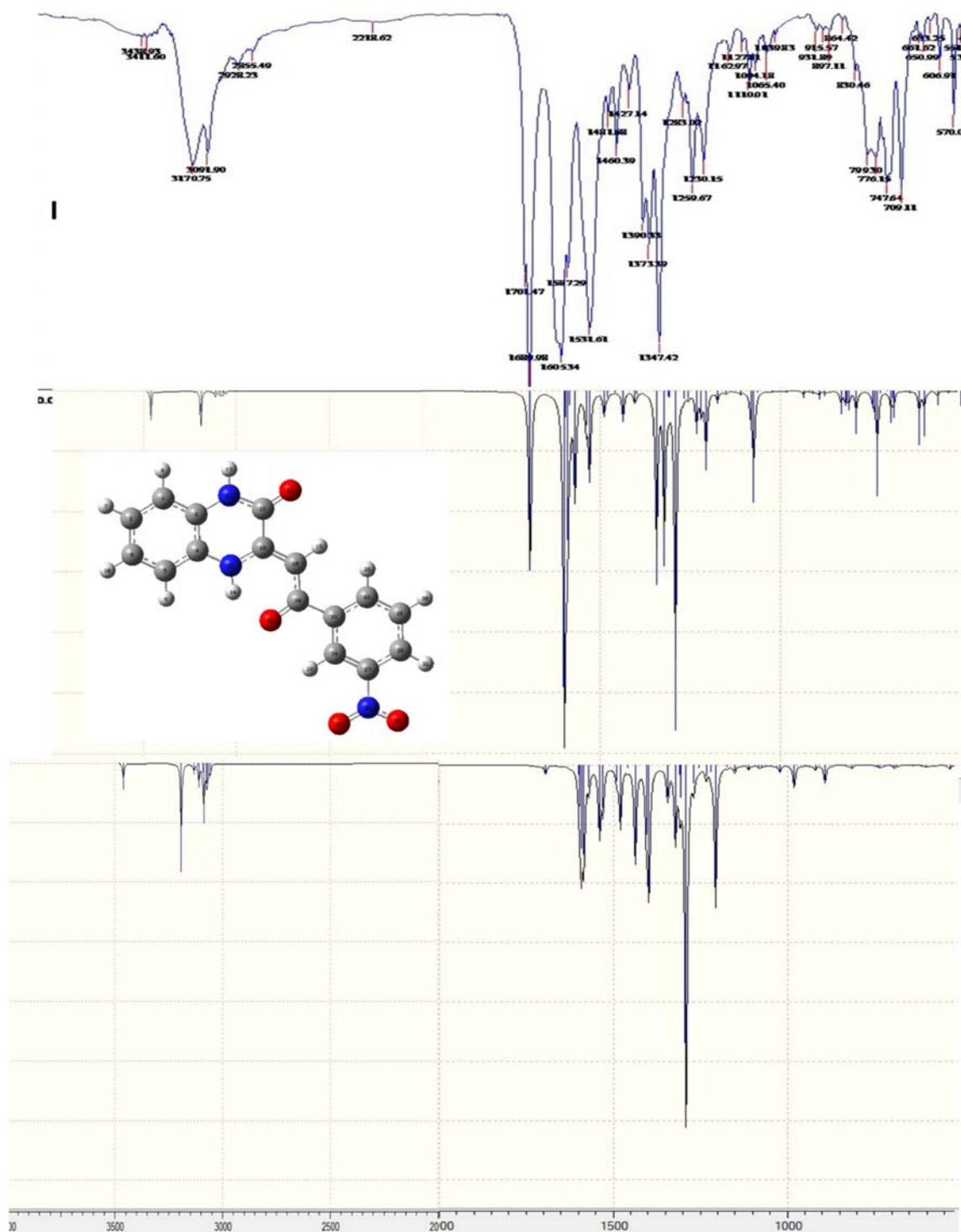
Figure 3. Experimental (a), calculated IR (b) and calculated Raman (c) for compound **3** (picture I) and compound **4** (picture II).

3.3 *Raman activities*

The results presented here are obtained using the laser with λ = 780 nm and the laser power level set to 10 mW. The experimental results were compared with theoretically predicted and simulated vibrations. C–H stretch vibration around 3000 cm^{-1} is missing only from spectra of compound **2** due to high noise in that range.[27] The bands around 1540 cm^{-1} and 1560 cm^{-1} in compounds **1–2** and
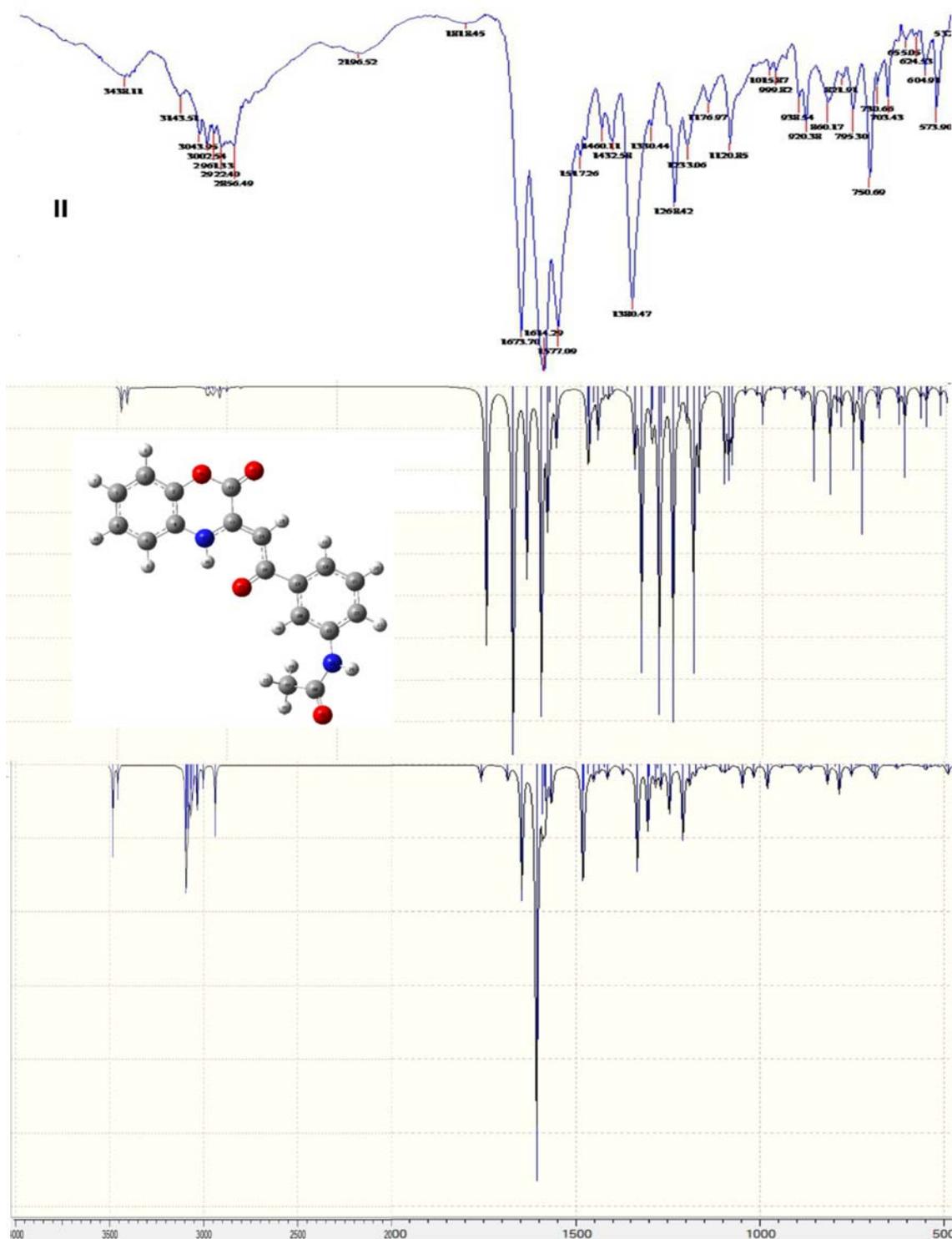
Figure 3. continued

compounds **3–4**, respectively, have been attributed to C–N–H vibrations. One of the peaks with the highest intensities in spectra of compounds **1–3** in the near 1330–1380 cm^{-1} arises from C–O stretching.[28] The strongest peak in spectra of compound **4** arises from the benzene ring oscillations, as theory predicts around 1500 cm^{-1} (in collected spectra 1498 cm^{-1}). Peaks in the region of 1235–1275 cm^{-1} correspond to the asymmetric bending of N–O bonds in the compounds. C–O–C symmetric stretch vibration modes[29] can be found at 1000–1050 cm^{-1} (Figures 4 and 5).

Collected Raman spectra for compound **3** have shown very low peak intensity and a lot of noise in the spectra. This may be explained with the morphology of the sample and the ratio of the crystallinity and the amorphous phase in the sample. Samples with higher crystallinity had higher peak intensities. Confirmation for this comes from the microscopy images taken during Raman spectroscopy analysis with Olympus light microscope coupled with 10 magnification objective (Figure 6).

The vibrations of the analyzed samples are well identified in the collected spectra within their characteristic regions and their calculated peak values coincide very well with the experimental values. Some differences between collected and calculated spectra can be observed. This is partly due to the approximate nature of the quantum mechanical models of vibration calculations. Also, some deviations of calculated wavenumbers compared to the experimental results can be attributed to the underestimation of the large degree of π-electron delocalization due to conjugation of the molecule.

3.4 *Electronic absorption analysis*

The absorption wavelengths correspond to the electronic transition from the ground to the first excited state. Electron absorption is described by one electron excitation from the highest occupied molecular orbital (HOMO) to the lowest unoccupied molecular orbital (LUMO). The frontier molecular orbitals and energy difference between HOMO and LUMO play an important role in the electric and optical properties. Common types of electronic transitions in organic molecules are π–π*, n–π* and π*(acceptor)–π (donor). The experimental UV spectrum of compound **1** is shown in Figure 7. The experimental absorption wavelengths (energies) and computed electronic values, such as absorption wavelengths (λ), excitation energies (E), oscillator strengths (f) and orbital description are tabulated in Table 3. HOMO and LUMO orbitals are of crucial importance in chemical reactions. The HOMO energy corresponds to the ability of electron giving while LUMO energy corresponds to the ability of electron-accepting. Difference between HOMO and LUMO energy (gap energy) characterizes the molecular chemical stability. The TD-DFT calculations were carried out using B3LYP/6-311+G(d,p) level of theory and solvation model CPCM[30] (ethanol solution). The results obtained here give insight into electron transitions from the ground state to excited state at the molecular orbital level.
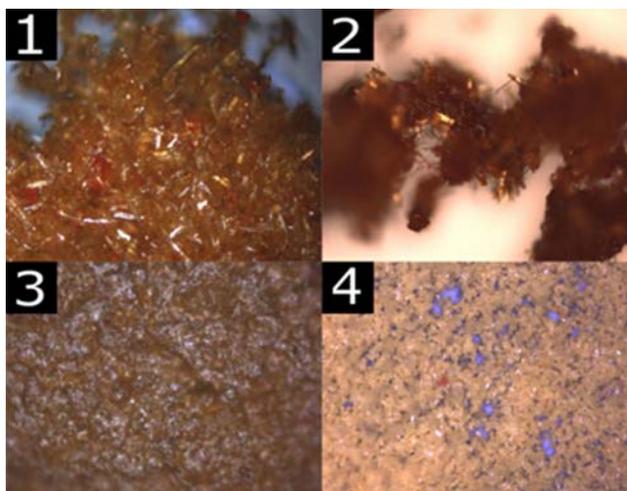
For compound **1** the absorption of UV radiation with a wavelength of 412 nm with an oscillator strength f = 0.95 induces the intramolecular electronic
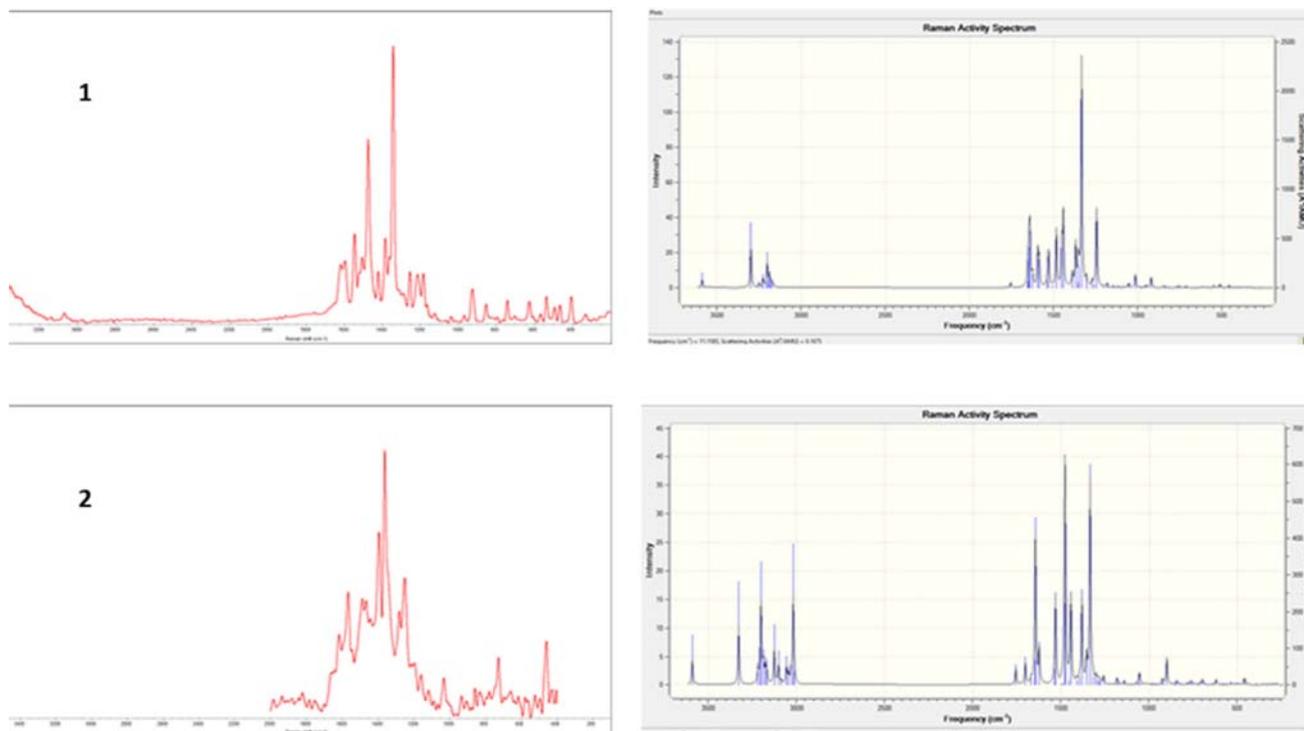
Figure 4. Experimental results of Raman spectroscopy of the compounds **1** and **2**.
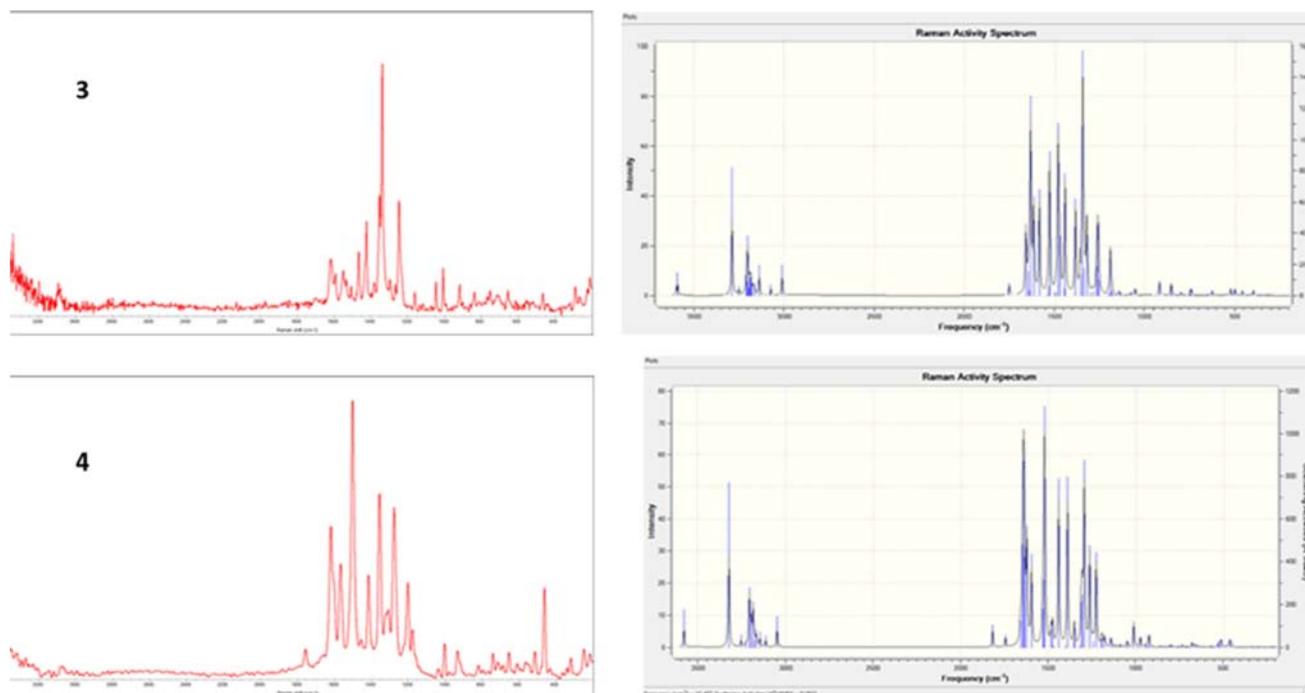
Figure 5. Experimental results of Raman spectroscopy of compounds **3** and **4**.


Figure 6. Microscopy images taken during Raman spectroscopy analysis.

transition n→π*. The other absorption band calculated at 228 nm with an oscillator strength f = 0.33 induces the intramolecular transition with n→π* and π→π* character. In consideration of calculated absorption spectra, the maximum absorption wavelength corresponds to the electronic transition from the HOMO to LUMO with 70% and from the HOMO to LUMO+1 also with 70% contribution. The frontier molecular orbitals (FMOs) for compound **1** are presented in Figure 8. For compounds **2**, **3** and **4** simulated UV-Vis spectra and HOMO-LUMO orbitals see

Supplementary Information. The simulated FMOs from Figure 8 indicates the presence of intramolecular charge transfer within the whole molecule. Similar charge transfer regarding the LUMO orbitals is obtained for compounds **3** and **4**, while in the case of compound **2** electron transfer is located on quinoxaline scaffold as a consequence of the absence of benzoyl fragment. Electron charge transfer concerning the HOMO orbitals for compounds **2–4** is distributed only through heterocyclic rings (Figures S4–S6, Supplementary Information).

In previously published papers it can be found that many of the organic compounds used as corrosion inhibitors are heterocyclic compounds that contain polar functional groups such as –OH, –OCH$_3$, –Cl, –NO$_2$, –CN, –C=N–, –CH$_3$, –NH$_2$, etc., or unsaturated (double and triple) bonds that can serve as adsorption centers due to the presence of π-electrons or non-bonding pair.[31–33] In most cases, the presence of electron-donating groups such as –OH, –NH$_2$, –CH$_3$, –OCH$_3$ etc., increases the inhibition performance because that group increases the electron density at the inhibitor's adsorption center and thus increase interactions between the inhibitor and the metallic surface. On the other hand, the presence of electron-withdrawing groups such as –NO$_2$, –CN, COOH, –COOC$_2$H$_5$ decreases the inhibition efficiency of organic molecules because that group decreases the
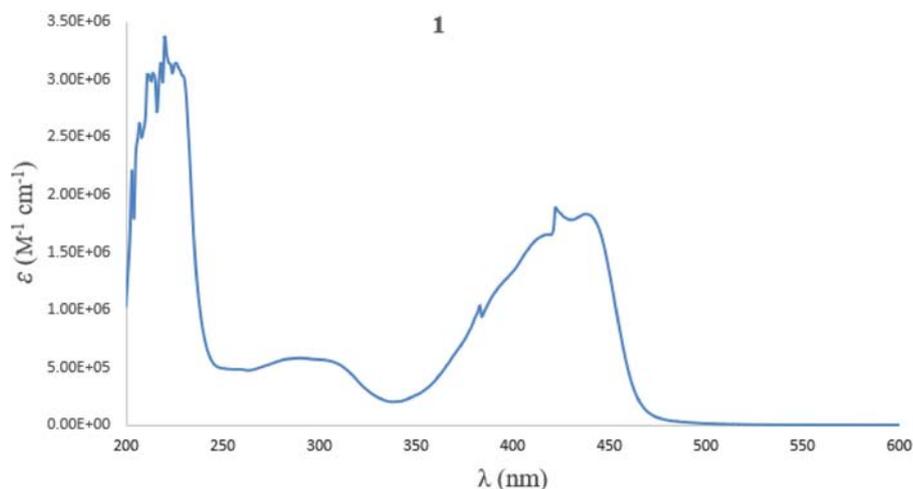
Figure 7. Experimental UV-Vis spectrum of compound **1**.

Table 3. Experimental and theoretical electronic absorption spectra of selected compounds (**1**, **2**, **3** and **4**) (absorption wavelength λ (nm), excitation energies E (eV) and oscillator strengths (f)) using TD-DFT/B3LYP/6-311+G(d,p) method in ethanol as solvent.

Compounds	Experimental λ (nm)	E (eV)	TD-DFT (B3LYP/6-311+G(d,p))			
			λ (nm)	E (eV)	f	Orbital description
1	422	2.93	412	3.00	0.95	H→L (70%)
	270	4.37	228	5.43	0.33	H-2→L+1 (61%)
2	400	3.09	377	3.28	0.59	H→L (70%)
	275	4.49	219	5.66	0.14	H-2→L+2 (58%)
3	425	2.87	417	2.97	0.78	H→L+1 (70%)
	260	4.74	270	4.58	0.06	H-4→L+1 (60%)
4	420	2.93	421	2.94	0.73	H→L (70%)
	255	4.81	228	5.42	0.11	H-2→L+1 (64%)

electron density at the adsorption center of the inhibitor leading to a decrease of the adsorption tendency on metallic surface.[34–36] With that purpose, we investigated the electronic parameters of selected compounds such as HOMO (E_{HOMO}) and LUMO (E_{LUMO}) energies, energy gap (ΔE), electronegativity (χ), dipole moment (μ), electron affinity (A), ionization potential (I), hardness (η), softness (σ), electron charge transfer (ΔN). Using the equations below[37], all these global molecular reactivity descriptors are estimated from the optimized structures (Table 4).

$$\Delta E_{gap} = E_{LUMO} - E_{HOMO} \tag{1}$$

$$I = -E_{HOMO} \tag{2}$$

$$A = -E_{LUMO} \tag{3}$$

$$\chi = \frac{I + A}{2} \tag{4}$$

$$\eta = \frac{I - A}{2} \tag{5}$$

$$\sigma = \frac{1}{\eta} \tag{6}$$

$$\Delta N = \frac{\chi(Fe) - \chi(inh)}{2(\eta(Fe) + \eta(inh))} \tag{7}$$

The values of χ (Fe) and η (Fe) are taken as 7 eV/mol and 0 eV/mol respectively. The calculations for compounds **1**, **2**, **3** and **4** show that compound **1** has the highest HOMO energy (−5.900 eV) and compound **4** the lowest LUMO energy at (−2.928 eV) compared to the calculated parameters for compounds **2** (−5.961 and −2.332) and **3** (−6.096 and −0.657 eV). These results indicate that compound **1** has higher inhibitory efficiency because it has been shown that higher the value of HOMO energy, the lesser is the value of the ionization potential, and the easier it is for the electrons to be donated.[38] The
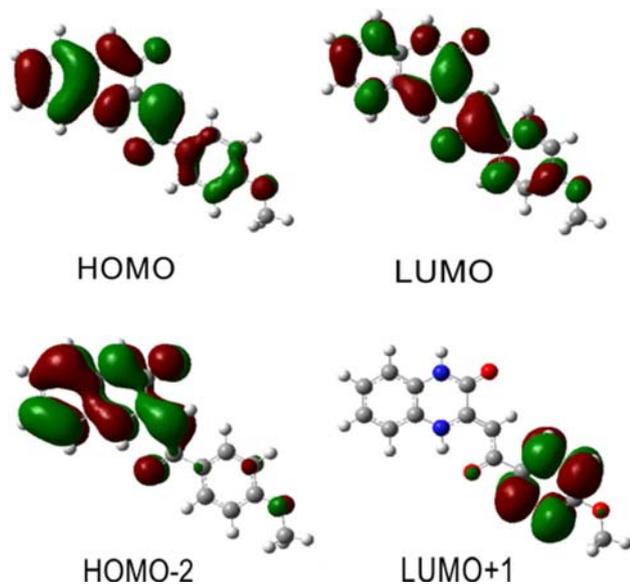
Figure 8. The frontier molecular orbitals for compound **1**.

reactivity tendency of the organic molecule towards the metal surface and electrical transport properties are determined by energy gap (ΔE). Low value of the energy gap will provide good inhibition efficiencies because the energy that is required to remove an electron from the last occupied orbital will be low. Also, the lower value of ΔE_{gap} means the higher stability for the formed complex on the metallic surface. The values of ΔE_{gap} for compounds **1**, **2**, **3** and **4** are 3.386, 3.629, 5.439 and 3.309 eV, respectively. Inhibitor **4** has lower energy gap than **1**, **2** and **3** and this means that the molecule could have better inhibition performance. The bandgap energy value of compound **3** was calculated as 5.439 eV, which confirms that the molecule has most stable structure compared to **1**, **2** and **4** and the ΔE_{gap} is comparable with the value of ΔE_{gap} some bioactive molecules.[39] The lower value of electron affinity (0.657 eV for compound **3**) shows that the mentioned molecule readily accepts electrons to form bonds; that means the higher molecular reactivity with nucleophiles.

Softness (σ) and absolute hardness (η) are important properties that are related to molecular stability and reactivity. In accordance with this, inhibition efficiency increases with increasing softness and decreases on increasing the hardness of the molecules.[40] In comparison with compounds **1** (η = 1.693 eV, σ = 0.591 eV^{-1}), **2** (η = 1.814 eV, σ = 0.551 eV^{-1}) and **3** (η = 2.720 eV, σ = 0.368 eV^{-1}) compound **4** has a lower hardness value (1.654 eV) and a higher value of softness (0.604 eV^{-1}).

ΔN is defined as an amount of charge transfer between the molecules and the mild steel surface. If ΔN has positive value then molecules have the ability to receive electrons, while a negative value of ΔN show that the molecules have the ability to donate electron.[41] In our case, all compounds have a positive value of ΔN suggesting that the investigated molecules possess charge transfer abilities towards mild steel.

Compounds **1** and **4** that contain electron-donating groups (–OCH_3, –$NHCOCH_3$) exhibit better inhibitory efficiency than compounds **2** and **3** that contain electron-withdrawing groups (–NO_2, alkenyl chain) that is in correlation with the previously published results.

3.5 ^1H and ^{13}C NMR spectra

The combination of experimental and theoretical studies could be a powerful and helpful tool for interpretation and prediction of molecular structures. Both ^1H and ^{13}C NMR spectra of selected compounds were previously recorded in DMSO, and all the ^1H NMR and ^{13}C NMR chemical shifts signals were assigned to the corresponding protons and carbons. In order to confirm these assignments, the ^1H and ^{13}C NMR spectra of the mentioned compounds were calculated using the GIAO method in DMSO with the CPCM solvation model at the B3LYP/6-311+G(d,p) level of theory. The experimental and calculated ^1H and ^{13}C NMR chemical shifts for compound **1** are presented in Table 5. For other compounds (**2–4**) see Supplementary Information. The atom positions were numbered as in the figure in Table 5. The isotropic chemical shifts are calculated with respect to tetramethylsilane (TMS) as standard. Calculated ^1H and ^{13}C isotropic chemical shifts were scaled with a single

Table 4. The quantum descriptors of compounds **1**, **2**, **3** and **4** calculated using DFT at B3LYP/6-311+G (d, p).

Parameter	E_{homo} (eV)	E_{lumo} (eV)	ΔE (eV)	A (eV)	I (eV)	χ (eV)	η (eV)	σ (eV^{-1})	ΔN
1	−5.900	−2.514	3.386	2.514	5.900	4.207	1.693	0.591	0.825
2	−5.961	−2.332	3.629	2.332	5.961	4.146	1.814	0.551	0.786
3	−6.096	−0.657	5.439	0.657	6.096	3.376	2.720	0.368	0.666
4	−6.237	−2.928	3.309	2.928	6.237	4.582	1.654	0.604	0.731

Table 5. Theoretical and experimental ^{1}H and ^{13}C isotropic chemical shifts for compound **1**.
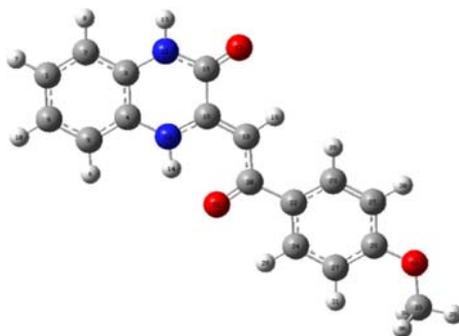
Atom	Experimental ^{13}C NMR	Theoretical-scaled chemical shifts (ppm)	Atom	Experimental ^{1}H NMR	Theoretical-scaled chemical shifts (ppm)
C1	115.6	123.8	H7	7.05	8.4
C2	114.2	114.9	H8	7.05	8.4
C3	129.4	125.0	H9	7.05	8.1
C4	116.4	126.1	H10	7.05	8.4
C5	114.2	114.4	H12	13.57	15.2
C6	115.6	123.2	H14	11.96	8.9
C15	145.2	142.9	H20	6.76	7.9
C16	156.1	154.0	H26	7.94	9.1
C18	89.2	89.3	H28	7.94	9.7
C19	188	184.6	H30	7.05	8.1
C22	131.6	130.5	H31	7.42	8.1
C23	124.5	128.6	H34	3.82	4.8
C24	126.7	129.4	H35	3.82	4.5
C25	123.9	115.7	H36	3.82	4.5
C27	116.4	108.9			
C29	162.6	162.3			
C33	55.6	55.3			

scaling factor of 1.1119 and 0.9409, respectively. These scaling factors are calculated using the least squares method. Taking into account that the range of ^{13}C NMR chemical shifts for a typical organic molecule in most cases occur >100 ppm[42] the accuracy confirms reliable of spectroscopic parameters. Chemical shifts for the carbon atoms that are part of the rings are >100 ppm, as expected. The signal of aromatic carbon atoms was observed at 115.6, 114.2, 129.4, 116.4, 131.6, 124.5 and 126.7 ppm which was calculated at 123.8, 114.9, 125.0, 126.1, 130.5, 128.6, 129.4 ppm.

Calculated ^{13}C isotropic chemical shifts match very well with experimental values with the correlation coefficients (r^2) of 0.9696 (**1**), 0.9910 (**2**), 0.9933 (**3**) and 0.9528 (**4**). In the case of calculated ^{1}H isotropic chemical shifts there are good agreements but for N–H chemical shifts a large deviation occurred. The agreement between the experimental and simulated N–H chemical shifts is moderate, probably because of intra- or intermolecular interactions (hydrogen bond) that have not appeared in simulated structure.

4. Conclusions

Quinoxalinone and benzoxazinone derivatives, as a very important class of compounds, were explored by spectroscopy (UV-Vis, IR, Raman and NMR) and theoretical study (DFT calculations) for better understanding of their structure and chemical properties. Also, quantum chemical parameters were calculated in order to investigate the corrosion inhibition properties of these molecules. Presented results confirmed the applicability of the used method and basis set for quinoxaline- and benzoxazine-based compounds. The theoretical UV-Vis spectra and calculated HOMO-LUMO orbitals are in agreement with experimental data. The positive value of ΔN suggests that investigated molecules possess charge transfer abilities

towards mild steel. Vibrational frequencies were calculated and compared with experimental values. A major source of some disagreement between the experimental and calculated band positions is the consequence of the fact that the calculations consider an isolated molecule and ignore intermolecular interactions. The vibrations of the analyzed samples are well identified in the collected Raman spectra within their characteristic regions and their calculated peak values coincide very well with the experimental values. Also, the values of the calculated chemical shifts for carbons notably are in excellent agreement with the experimental values. That is not the case, with chemical shifts for hydrogen atoms. There are some deviations for N–H chemical shifts, probably because of the formation of hydrogen bond between two scaffolds (intermolecular interactions) or N–H amine and carbonyl group from aryl or alkyl fragment (intramolecular interactions).

Supplementary Information (SI)

^{1}H NMR, ^{13}C NMR (experimental and theoretical), experimental UV-Vis and HOMO-LUMO data are submitted as Supplementary Information. Supplementary Information is available on www.ias.ac.in/chemsci.

Acknowledgements

Conflict of interest The authors have declared no conflicts of interest.

References

1. Ramli Y, Moussaif A, Karrouchi K and Essassi E M 2014 Pharmacological profile of quinoxalinone *J. Chem.* **2014** ID 563406
2. Pereira J A, Pessoa A M, Cordeiro M N, Fernandes R, Prudêncio C, Noronha J P and Vieira M 2015 Quinoxaline, its derivatives and applications: A State of the Art review *Eur. J. Med. Chem.* **97** 664
3. Blattes E, Lockhart B, Lestage P, Schwendimann L, Gressens P, Fleury M B and Largeron M 2005 Novel 2-alkylamino-1,4-benzoxazine derivatives as potent neuroprotective agents: Structure-activity relationship studies *J. Med. Chem.* **48** 1282
4. Ismail M, Amin K, Noaman E, Soliman D and Ammar Y 2010 New quinoxaline 1,4-di-N-oxides: Anticancer and hypoxia-selective therapeutic agents *Eur. J. Med. Chem.* **45** 2733
5. Chitra S, Parameswari K, Vidhya M, Kalishwari M and Selvaraj A 2011 Evaluation of quinoxalines as corrosion inhibitors for mild steel in acid environment *Int. J. Electrochem. Sci.* **6** 4593
6. Thomas K R J, Lin J T, Tao Y T and Chuen C H 2002 Quinoxalines incorporating triarylamines: potential electroluminescent materials with tunable emission characteristics *Chem. Mater.* **14** 2796
7. Obi-Egbedi N O, Obot I B and El-Khaiary M I 2011 Quantum chemical investigation and statistical analysis of the relationship between corrosion inhibition efficiency and molecular structure of xanthene and its derivatives on mild steel in sulphuric acid *J. Mol. Struct.* **1002** 86
8. Zarrouk A, Zarrok H, Salghi R, Hammouti B, Al-Deyab S S, Touzani R, Bouachrine M, Warad I and Hadda T B 2012 A Theoretical investigation on the corrosion inhibition of copper by quinoxaline derivatives in nitric acid solution *Int. J. Electrochem. Sci.* **7** 6353
9. El-Hajjaji F, Zerga B, Sfaira M, Taleb M, Ebn Touhami M, Hammouti B, Al- Deyab S S, Benzeid H and Essassi E M 2014 Comparative study of novel N-substituted quinoxaline derivatives towards mild steel corrosion in hydrochloric acid: Part 1 *J. Mater. Environ. Sci.* **5** 255
10. Fu J J, Zang H S, Wang Y, Li S N, Chen T and Liu X D 2012 Experimental and theoretical study on the inhibition performances of quinoxaline and its derivatives for the corrosion of mild steel in hydrochloric acid *Ind. Eng. Chem. Res.* **51** 6377
11. Zarrouk A, Hammouti B, Dafali A, Bouachrine M, Zarrok H, Boukhris S and Al-Deyab S S 2014 A theoretical study on the inhibition efficiencies of some quinoxalines as corrosion inhibitors of copper in nitric acid *J. Saudi. Chem. Soc.* **18** 450
12. Adardour K, Touir R, Ramli Y, Belakhmima R A, Ebn Touhami M, Mubengayi C K, Kafsaoui E H and Essassi E M 2013 Comparative inhibition study of mild steel corrosion in hydrochloric acid by new class synthesised quinoxaline derivatives: Part I *Res. Chem. Intermed.* **39** 1843
13. Petronijević J, Bugarčić Z, Bogdanović G A, Stefanović S and Janković N 2017 An enolate ion as a synthon in biocatalytic synthesis of 3,4-dihydro-2(1H)-quinoxalinones and 3,4-dihydro-1,4-benzoxazin-2-ones: lemon juice as an alternative to hazardous solvents and catalysts *Green Chem.* **19** 707
14. Ayaza M, Dietricha J and Hulme C 2011 A novel route to synthesize libraries of quinoxalines via Petasis methodology in two synthetic operations *Tetrahedron Lett.* **52** 4821
15. Palafox M A and Rastogi V K 2011 Vibrational spectra, tautomerism and thermodynamics of anticarcinogenic drug: 5-Fluorouracil *Spectrochim. Acta A Mol. Biomol. Spectrosc.* **79** 970
16. Devlin F J, Finley J W, Stephens P J and Frisch M J 1995 Ab initio calculation of vibrational absorption and circular dichroism spectra using density functional force fields: A comparison of local, nonlocal, and hybrid density functionals *J. Phys. Chem.* **99** 16883
17. Seminario J M 1995 In *Modern Density Functional Theory: A Tool for Chemistry* P Politzer (Ed.) (Amsterdam: Elsevier) p. 49

18. Becke A D 1992 Density-functional thermochemistry. II. The effect of the Perdew–Wang generalized-gradient correlation correction *J. Chem. Phys.* **97** 9173; and 1993 Density-functional thermochemistry. III. The role of exact exchange *J. Chem. Phys.* **98** 5648

19. Lee C, Yang W and Parr R G 1988 Development of the Colle-Salvetti correlation-energy formula into a functional of the electron density *Phys. Rev. B* **37** 785

20. Krishnan R, Binkley J S, Seeger R and Pople J A 1980 Self-consistent molecular orbital methods. XX. A basis set for correlated wave functions *J. Chem. Phys.* **72** 650

21. Gaussian 09, Revision C.01, Frisch M J, Trucks G W, Schlegel H B, Scuseria G E, Robb M A, Cheeseman J R, Scalmani G, Barone V, Mennucci B, Petersson G A, Nakatsuji H, Caricato M, Li X, Hratchian H P, Izmaylov A F, Bloino J, Zheng G, Sonnenberg J L, Hada M, Ehara M, Toyota K, Fukuda R, Hasegawa J, Ishida M, Nakajima T, Honda Y, Kitao O, Nakai H, Vreven T, Montgomery J A, Peralta J E, Ogliaro F, Bearpark M, Heyd J J, Brothers E, Kudin K N, Staroverov V N, Keith T, Kobayashi R, Normand J, Raghavachari K, Rendell A, Burant J C, Iyengar S S, Tomasi J, Cossi M, Rega N, Millam J M, Klene M, Knox J E, Cross J B, Bakken V, Adamo C, Jaramillo J, Gomperts R, Stratmann R E, Yazyev O, Austin A J, Cammi R, Pomelli C, Ochterski J W, Martin R L, Morokuma K, Zakrzewski V G, Voth G A, Salvador P, Dannenberg J J, Dapprich S, Daniels A D, Farkas O, Foresman J B, Ortiz J V, Cioslowski J and Fox D J 2010 Gaussian, Inc., Wallingford CT

22. Andersson M P and Uvdal P 2005 New scale factors for harmonic vibrational frequencies using the B3LYP density functional method with the triple-zeta basis set 6−311+G(d,p) *J. Phys. Chem. A* **109** 2937

23. Wolinski K, Hilton J F and Pulay P 1990 Efficient implementation of the Gauge-Independent Atomic Orbital method for NMR chemical shift calculations *J. Am. Chem. Soc.* **112** 8251

24. Silverstein R M, Webster F X and Kiemle D J 2005 In *Spectrometric Identification of Organic Compounds* (London: John Willey) p. 72

25. Babu N R, Subashchandrabose S, Padusha M S A, Saleem H, Manivannan V and Erdogdu Y 2014 Synthesis and structural characterization of (E)-N′- ((Pyridin-2-yl) methylene) benzohydrazide by X-ray diffraction, FT-IR, FT-Raman and DFT methods *J. Mol. Struct.* **1072** 84

26. Weinhold F 2005 In *Valency and bonding: a natural bond orbital donor-acceptor perspective* C R Landis (Ed.) (Location: Cambridge University Press) p. 367

27. Krishnakumar V and Muthunatesan S 2007 DFT studies of the structure and vibrational assignments of 4-hydroxy quinazoline and 2-hydroxy benzimidazole *Spectrochim. Acta Part A* **66** 1082

28. Krishnakumar V, Mathammal R and Muthunatesan S 2008 Structures and vibrational frequencies of 2-naphthoic acid and 6-bromo-2-naphthoic acid based on density functional theory calculations *Spectrochim. Acta Part A* **70** 201

29. Schrader B (Ed.) 1995 In *Infrared and Raman Spectroscopy: Methods and Applications* (Germany: Wiley-VCH Verlag GmbH) p. 191

30. Tomasi J, Mennucci B and Cammi R 2005 Quantum mechanical continuum solvation models *Chem. Rev.* **105** 2999

31. Umoren S A, Ogbobe O, Igwe I O and Ebenso E E 2008 Inhibition of mild steel corrosion in acidic medium using synthetic and naturally occurring polymers and synergistic halide additives *Corros. Sci.* **50** 1998

32. Gupta R K, Malviya M, Verma C and Quraishi M A 2017 Aminoazobenzene and diaminoazobenzene functionalized graphene oxides as novel class of corrosion inhibitors for mild steel: Experimental and DFT studies *Mater. Chem. Phys.* **198** 360

33. Verma C, Ebenso E E and Quraishi M A 2017 Ionic liquids as green and sustainable corrosion inhibitors for metals and alloys: An overview *J. Mol. Liq.* **233** 403

34. Yadav M, Sinha R R, Kumar S and Sarkar T K 2015 Corrosion inhibition effect of spiropyrimidinethiones on mild steel in 15% HCl solution insight from: electrochemical and quantum studies *RSC Adv.* **5** 70832

35. Harvey T G, Hardin S G, Hughes A E, Muster T H, White P A, Markley T A, Corrigan P A, Mardel J, Garcia S J, Mol J M C and Glenn A M 2011 The effect of inhibitor structure on the corrosion of AA2024 and AA7075 *Corros. Sci.* **53** 2184

36. Sagdinc S G and Kara Y S 2014 Theoretical elucidation on corrosion inhibition efficiency of 11-cyano undecanoic acid phenylamide derivatives: DFT study *Prot. Metal. Phys. Chem. Surf.* **50** 111

37. Bouoidina A, Hajjaji E F, Abdellaoui A, Rais Z, Filali Baba M, Chaouch M, Karzazi O, Lahkimi A and Taleb M 2017 Theoretical and experimental study of the corrosion inhibition of mild steel in acid medium using some surfactants of the essential oil of FoeniculumVulgare bulb *J. Mater. Environ. Sci.* **8** 1328

38. Awad M K 2013 Quantum chemical studies and molecular modeling of the effect of polyethylene glycol as corrosion inhibitors of an aluminum surface *Can. J. Chem.* **91** 283

39. Costa R A, Oliveira K M T, Costa E V and Pinheiro M L B 2017 Vibrational, structural and electronic properties investigation by DFT calculations and molecular docking studies with DNA topoisomerase II of strychnobrasiline type alkaloids: a theoretical approach for potentially bioactive molecules *J. Mol. Struct.* **1145** 254

40. Obot I B and Gasem Z M 2014 Theoretical evaluation of corrosion inhibition performance of some pyrazine derivatives *Corros. Sci.* **83** 359

41. Kovacevic N and Kokalj A 2011 DFT study of interaction of azoles with Cu(III) and Al(III) Surfaces: role of azole nitrogen atoms and dipole-dipole interactions *J. Phys. Chem. C* **115** 24189

42. Kalinowski H O, Berger S and Braun S 1988 Carbon-13 NMR Spectroscopy (Chichester: John Wiley & Sons) p. 512